On Homogenization of Fiber-Reinforced Polymers

Changyou Li and Dominique Lesselier

Abstract – The purpose of this article is to get equivalent constitutive parameters of fiber-reinforced polymers with periodic arrangements of fibers via homogenization. The homogenized structure is used to replace the original one to speed up field calculations without losing much accuracy. A rigorous derivation is sketched, and computational accuracy for lossy and lossless materials is exhibited for transverse electric and transverse magnetic impinging waves, validation being provided by a semianalytical approach.

1. Introduction

Fiber-reinforced polymers have many applications in aerospace [1, 2] and other industries [3, 4]. In particular, they offer low weight and high stiffness. They are typically composed of a binding matrix reinforced by long fibers with different properties (e.g., carbon or glass fibers), the organization of the microstructure influencing the macroscopic behavior.

Accurate numerical methods have been developed to study the electromagnetic properties of such composites, and their imaging, whenever they are damaged. The surface integral equation method [5], the finite difference time domain (FDTD) method [6], or the finite element method (FEM) [7] can be run with a periodic boundary condition applied. Yet FDTD and FEM require a very fine discretization of the fibers, which tends to be computationally prohibitive even at low frequency of operation. As for the surface integral equation method, it requires the periodic Green's function and faces convergence [8].

So, an efficient approach to parametrize properties of composites with small cost is of interest. A rigorous method for fiber-reinforced laminates with arbitrary orientation of fibers in different layers [9] ensures computational efficiency and accuracy and analytic tractability as well, such as for woodpiles. Based on the periodic distribution of fibers within each layer, lattice sums arise. Yet those converge poorly when the matrix material is lossless, while the method works only for circular cylindrical fibers.

Several approximation methods valid at low enough frequency are in the literature. The equivalent-layer method [10] shows good potential. It replaces specific composites by a homogeneous equivalent slab material. The approach models anisotropy and arbitrary polarization with arbitrary angles of incidence. A transmission line model [12] is effective for single- and multilayered thin panels and can be used to investigate carbon fiber–reinforced panels. Yet in both cases, relative permittivities and permeabilities have to be derived for different structures. Here, an asymptotic homogenization is carried out. A periodic single layer is replaced with a single layer with equivalent permittivity and permeability. Primary investigations are in [11]. Simulations for lossless and lossy fiber-reinforced polymers are shown to fasten the computations without too much loss of accuracy.

Manuscript received 25 December 2021.

Changyou Li is with the Department of Electric Engineering, School of Electronics and Information, Northwestern Polytechnical University, Xi'an, 710029 Shaanxi, China; e-mail: changyou.li@nwpu.edu.cn.

Dominique Lesselier is with the Université Paris-Saclay, CNRS, CentraleSupélec, Laboratoire des signaux et systèmes, 91190 Gif-sur-Yvette, France; e-mail: dominique.lesselier@centralesupelec.fr.

2. Homogenization Procedure

The analytical model of one single-layer polymer reinforced by a periodic array of circular fibers has been given in [9]. Here, the fiber-reinforced slab is replaced by its uniaxially anisotropic counterpart with an effective permittivity tensor. Under illumination by a transverse electric (TE) or transverse magnetic (TM) polarized wave, only a scalar effective permittivity is needed. The geometry is sketched in Figure 1 with upper and lower boundaries at $z = a$ and b. The periodic direction is along the x axis, and the periodic unit is the region between the two dashed lines with width d. The area of the unit cell is $S = S_1 + S_2$, where S_1 and S_2 are occupied by the matrix and by the fiber with arbitrary cross section, respectively. Relative permittivities in S_1 and S_2 are ε_{r1} and ε_{r2}, respectively.

In isotropic inhomogeneous media, one has $\nabla \times \mathcal{E} = i\omega\mu\mathcal{H}$ and $\nabla \times \mathcal{H} = -i\omega\varepsilon\mathcal{E}$, and $\mathcal{E}$ and $\mathcal{H}$ are electric and magnetic fields, respectively. $\mathcal{E} = E_x\vec{x} + E_y\vec{y} + E_z\vec{z}$, $\mathcal{H} = H_x\vec{x} + H_y\vec{y} + H_z\vec{z}$, permeability $\mu = \mu_0$, μ_0 as free space permeability, permittivity $\varepsilon = \varepsilon_r\varepsilon_0$, ε_0 as free space permittivity, where ε_r varies with x and z, and is written as $\varepsilon_r(x, z)$. Letting the plane of incidence parallel with the x-z plane and with $k_0 = \omega\sqrt{\varepsilon_0\mu_0}$, one gets

$$\left(\nabla^2 + k_0^2\varepsilon_r\right)E_y = 0 \tag{1a}$$

$$\frac{\partial}{\partial x}\left(\frac{1}{\varepsilon_r}\frac{\partial H_y}{\partial x}\right) + \frac{\partial}{\partial z}\left(\frac{1}{\varepsilon_r}\frac{\partial H_y}{\partial z}\right) + k_0^2 H_y = 0 \tag{1b}$$

With these two wave equations, the periodic composite can be homogenized at a low enough frequency, meaning that the composite is replaced by a homogeneous slab with effective permittivity $\bar{\varepsilon}_r$ for the E-polarized incident wave (TM) case and the H-polarized one (TE).

Assuming a circular frequency ω such that $\lambda = \frac{2\pi c_0}{\omega} \gg d$ and c_0 is speed of light, the incident wavenumber $k_0 = \omega/c_0$ satisfies $k_0 \ll 1$. To obtain the

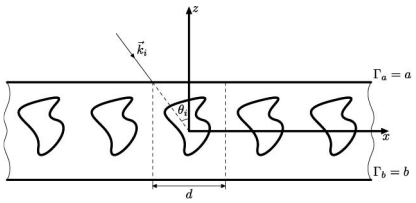

Figure 1. Single-layer fiber-reinforced polymer.

effective permittivities for TE and TM waves, one takes $E_y(x,z) = \tilde{E}_y(x,z,\tilde{x},\tilde{z})$ and $H_y(x,z) = \tilde{H}_y(x,z,\tilde{x},\tilde{z})$, where $\tilde{x} = k_0 x$ and $\tilde{z} = k_0 z$. Then ∇ and ∇^2 become

$$\nabla = \nabla_{x,z} + k_0 \nabla_{\tilde{x},\tilde{z}} \tag{2a}$$

$$\nabla^2 = \nabla^2_{x,z} + k_0^2 \nabla^2_{\tilde{x},\tilde{z}} + k_0(\nabla_{x,z} \cdot \nabla_{\tilde{x},\tilde{z}} + \nabla_{\tilde{x},\tilde{z}} \cdot \nabla_{x,z}) \tag{2b}$$

$\nabla_{x,z} = \frac{\partial}{\partial x}\vec{x} + \frac{\partial}{\partial z}\vec{z}$, and $\nabla^2_{x,z} = \frac{\partial^2}{\partial x^2} + \frac{\partial^2}{\partial z^2}$. $\nabla_{\tilde{x},\tilde{z}}$ and $\nabla^2_{\tilde{x},\tilde{z}}$ have similar definitions, but the operations are on $\tilde{x}$ and $\tilde{z}$.

With TE, applying (2b) to (1a), one has

$$\frac{1}{k_0^2}\nabla^2_{x,z}\tilde{E}_y + \frac{1}{k_0}(\nabla_{x,z} \cdot \nabla_{\tilde{x},\tilde{z}} + \nabla_{\tilde{x},\tilde{z}} \cdot \nabla_{x,z})\tilde{E}_y + \nabla^2_{\tilde{x},\tilde{z}}\tilde{E}_y + \varepsilon_r \tilde{E}_y = 0 \tag{3}$$

The electric field $\tilde{E}_y$ is then expanded as

$$\tilde{E}_y = \tilde{E}_{0y} + k_0 \tilde{E}_{1y} + k_0^2 \tilde{E}_{2y} + \cdots \tag{4}$$

Since k_0 is assumed small enough, the higher the order of the terms, the less the influence on $\tilde{E}_y$. Here, the first three are taken. Collecting terms with the same k_0 integer power yields

$$\begin{aligned}&\frac{1}{k_0^2}\nabla^2_{x,z}\tilde{E}_{0y} + \frac{1}{k_0}\left[\nabla^2_{x,z}\tilde{E}_{1y} + (\nabla_{x,z} \cdot \nabla_{\tilde{x},\tilde{z}} + \nabla_{\tilde{x},\tilde{z}} \cdot \nabla_{x,z})\tilde{E}_{0y}\right] \\ &+ \nabla^2_{x,z}\tilde{E}_{2y} + (\nabla_{x,z} \cdot \nabla_{\tilde{x},\tilde{z}} + \nabla_{\tilde{x},\tilde{z}} \cdot \nabla_{x,z})\tilde{E}_{1y} \\ &+ \nabla^2_{\tilde{x},\tilde{z}}\tilde{E}_{0y} + \epsilon_r \tilde{E}_{0y} = 0\end{aligned} \tag{5}$$

Setting to zero the terms at each integer power of k_0 yields

$$\nabla^2_{x,z}\tilde{E}_{0y} = 0 \tag{6a}$$

$$\nabla^2_{x,z}\tilde{E}_{1y} + (\nabla_{x,z} \cdot \nabla_{\tilde{x},\tilde{z}} + \nabla_{\tilde{x},\tilde{z}} \cdot \nabla_{x,z})\tilde{E}_{0y} = 0 \tag{6b}$$

$$\nabla^2_{x,z}\tilde{E}_{2y} + (\nabla_{x,z} \cdot \nabla_{\tilde{x},\tilde{z}} + \nabla_{\tilde{x},\tilde{z}} \cdot \nabla_{x,z})\tilde{E}_{1y} + \nabla^2_{\tilde{x},\tilde{z}}\tilde{E}_{0y} + \varepsilon_r \tilde{E}_{0y} = 0 \tag{6c}$$

Because of periodicity, $\tilde{E}_{0y}$ can be expanded as

$$\tilde{E}_{0y} = \sum_{p\in\mathbb{Z}} C_p(z) e^{i\alpha_p x} \tag{7}$$

where $\alpha_p = k_0 \sin\theta_i + 2\pi p/d$. Substituting (7) into (6a),

$$\frac{d^2 C_p}{dz^2} - \alpha_p^2 C_p = 0 \tag{8}$$

If $p \neq 0$, $C_p(z) = a_1 e^{\alpha_p z} + a_2$, where a_1 and a_2 are all constant. If $a_1 \neq 0$, there are only outgoing waves existing in both regions $z > 0$ and $z < 0$, which is not true, so $C_p = a_2$. Substituting it into (8), one gets that $a_2 = 0$, so $C_p = 0$. If $p = 0$, C_0 is constant. So, (6b) becomes

$$\nabla^2_{x,z}\tilde{E}_{1y} = 0 \tag{9}$$

the same solution as (6a). Simplifying (6c) produces

$$\nabla^2_{x,z}\tilde{E}_{2y} + \nabla^2_{\tilde{x},\tilde{z}}\tilde{E}_{0y} + \varepsilon_r \tilde{E}_{0y} = 0 \tag{10}$$

We expand $\tilde{E}_{2y}$ as

$$\tilde{E}_{2y} = \sum_{p\in\mathbb{Z}} C_p(z) e^{i\alpha_p x} \tag{11}$$

with which (10) is written as

$$\frac{d^2 C_p}{dz^2} - \alpha_p^2 C_p + \nabla^2_{\tilde{x},\tilde{z}}\tilde{E}_{0y} + \varepsilon_r(x,z)\tilde{E}_{0y} = 0 \tag{12}$$

If $p \neq 0$, this equation has a solution $C_p = a_1 e^{\alpha_p z} + f$, where f is a particular solution of (12). If $a_1 \neq 0$, the field in space $z > 0$ is infinite and in $z < 0$ is evanescent. If $p = 0$, (12) becomes

$$\frac{d^2 C_0}{dz^2} + \nabla^2_{\tilde{x},\tilde{z}}\tilde{E}_{0y} + \varepsilon_r(x,z)\tilde{E}_{0y} = 0 \tag{13}$$

Here, we have a solution of $C_0 = a_1 z^2 + a_2 z + a_3$. If $a_1 \neq 0$ and $a_2 \neq 0$, the field is infinite when $z = \infty$, so C_0 is constant. Then (13) becomes

$$\nabla^2_{\tilde{x},\tilde{z}}\tilde{E}_{0y} + \varepsilon_r(x,z)\tilde{E}_{0y} = 0 \tag{14}$$

Equation (14) provides a homogenized equation associated with the macroscopic behavior. To get the homogenized permittivity, the mean operator on S is introduced, denoted as $< \cdot >$. It acts on function g for variables x and y:

$$< g > = \frac{1}{S}\int\int_S g(x,y)dxdy \tag{15}$$

Applying the mean operator to both sides of (14), the left-hand side becomes

$$\begin{aligned}&\frac{1}{S}\int_{-d/2}^{d/2}\int_b^a (\nabla^2_{\tilde{x},\tilde{z}}\tilde{E}_{0y} + \varepsilon_r(x,z)\tilde{E}_{0y})dxdz \\ &= \nabla^2_{\tilde{x},\tilde{z}}\tilde{E}_{0y} + \frac{1}{S}\int_{-d/2}^{d/2}\int_b^a \varepsilon_r(x,z)dxdz\tilde{E}_{0y} \\ &= \nabla^2_{\tilde{x},\tilde{z}}\tilde{E}_{0y} + \bar{\varepsilon}_r\tilde{E}_{0y}\end{aligned} \tag{16}$$

with

$$\bar{\varepsilon}_r = \frac{1}{S}\int_{-d/2}^{d/2}\int_b^a \varepsilon_r(x,z)dxdz = \frac{\varepsilon_{r1}S_1 + \varepsilon_{r2}S_2}{S_1 + S_2} \tag{17}$$

A Helmholtz wave equation follows as

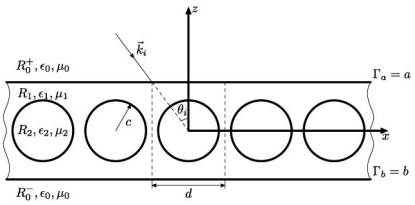

Figure 2. Single-layer fiber-reinforced polymer.

$$\nabla^2_{\tilde{x},\tilde{z}} \tilde{E}_{0y} + \bar{\varepsilon}_r \tilde{E}_{0y} = 0 \tag{18}$$

Since $\frac{\partial \tilde{E}_{0y}}{\partial \tilde{x}} = \frac{1}{k_0} \frac{\partial \tilde{E}_{0y}}{\partial x}$, (18) can be written as

$$\nabla^2_{x,z} \tilde{E}_{0y} + \bar{\varepsilon}_r k_0^2 \tilde{E}_{0y} = 0$$

indicating that $\bar{\varepsilon}_r$ is the effective permittivity with which the scattering of a low-frequency TM wave by the periodic composite is assimilated with the one of a homogeneous slab with permittivity $\bar{\varepsilon}_r$.

For an H-polarized incident wave, (1b) is needed. Allowing $\varepsilon_r^{-1}(x,z) = 1/\varepsilon_r(x,z)$, (1b) is expressed as

$$\frac{\partial}{\partial x}\left(\varepsilon_r^{-1}(x,z)\frac{\partial H_y}{\partial x}\right) + \frac{\partial}{\partial z}\left(\varepsilon_r^{-1}(x,z)\frac{\partial H_y}{\partial z}\right) + k_0^2 H_y = 0 \tag{19}$$

It can be expanded as

$$\varepsilon_r^{-1}\frac{\partial^2 H_y}{\partial x^2} + \varepsilon_r^{-1}\frac{\partial^2 H_y}{\partial z^2} + \frac{\partial H_y}{\partial x}\frac{\partial \varepsilon_r^{-1}}{\partial x} + \frac{\partial H_y}{\partial z}\frac{\partial \varepsilon_r^{-1}}{\partial z} + k_0^2 H_y = 0 \tag{20}$$

Noticing that $\varepsilon_r^{-1}(x,z)$ in regions R_1 and R_2 are all constant, the derivative of $\varepsilon_r^{-1}(x,z)$ with respect to x or z equals zero. Now (20) can be simplified as

$$\varepsilon_r^{-1}\nabla^2 H_y + k_0^2 H_y = 0 \tag{21}$$

Letting $H_y(x,z) = \tilde{H}_y(x,z,\tilde{x},\tilde{z})$ and expanding,

$$\tilde{H}_y = \tilde{H}_{0y} + k_0 \tilde{H}_{1y} + k_0^2 \tilde{H}_{2y} + \cdots \tag{22}$$

Then, as for the TM wave,

$$\varepsilon_r^{-1}\nabla^2_{\tilde{x},\tilde{z}} \tilde{H}_{0y} + \tilde{H}_{0y} = 0 \tag{23}$$

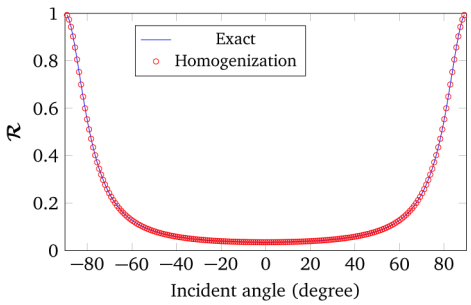

Figure 3. Reflection coefficients of GFRP, $L = d = 0.1$ mm, $c = 0.25d$, 60 GHz, TM.

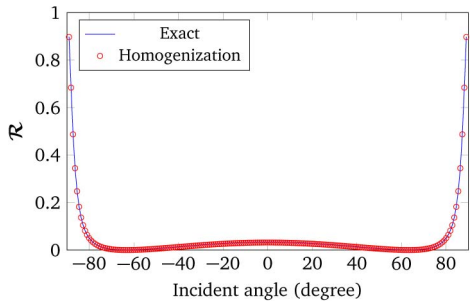

Figure 4. Reflection coefficients of GFRP, $L = d = 0.1$ mm, $c = 0.25d$, 60 GHz, TE.

The TE effective permittivity is calculated as

$$\bar{\varepsilon}_r = \frac{S_1 + S_2}{S_1/\varepsilon_{r1} + S_2/\varepsilon_{r2}} \tag{24}$$

3. Numerical Validation and Investigation

A single-layer circular fiber–reinforced polymer is studied for both TM and TE (Figure 2). One circular fiber is embedded into one unit cell, periodically repeated along x. Numerical results are obtained with the asymptotic homogenization and compared with those yielded by the analytically accurate plane wave expansion method [9].

A glass fiber ($\varepsilon_r^{(2)} = 6$)–reinforced ($\varepsilon_r^{(1)} = 3.6$) slab (GFRP with epoxy matrix) is first considered for TM and TE illumination. Effective permittivities are scalar, denoted as $\bar{\varepsilon}_r^{(tm)}$ and $\bar{\varepsilon}_r^{(te)}$, respectively. Since the structure is lossless, those are frequency independent. With $L = d = 0.1$ mm and $c = 0.25d$, effective permittivities are $\bar{\varepsilon}_r^{(tm)} = 4.0712$ and $\varepsilon_r^{(te)} = 3.9068$.

For obliquely incident waves, reflection coefficients varying with the angle of incidence are given in Figures 3 and 4 for TM and TE waves, respectively, impinging on a GFRP at 60 GHz. Exact results and those with the homogenized slab match well, with largest relative errors of 0.12% and 0.9%, respectively, for TM and TE waves.

Now consider a carbon fiber–reinforced polymer with $L = d = 0.1$ mm and $c = 0.25d$ (with epoxy matrix). Since the fibers are lossy, the effective permittivities, as given by the formulas above, vary with frequency. With them, power reflection and transmission coefficients can be calculated for the homogenized slab and results compared with exact values by the approach in [9]; see Figure 5 for the TM wave and Figure 6 for the TE wave. Results with the homogenized slab match exact values quite well for TM. The highest relative error is less than 0.3%. Good results are also obtained for TE, with a highest relative error of 4% at high frequency.

Corresponding power reflection and transmission coefficients vs. angle of incidence are shown in Figures 7 and 8 for TM and TE waves, respectively. Frequency is 60 GHz. Good matches are observed for TM. But if a clear difference is observed for TE, the largest relative error is less than 4%. In effect, $\Im\bar{\epsilon}_r^{te}$ can be shown to be very small

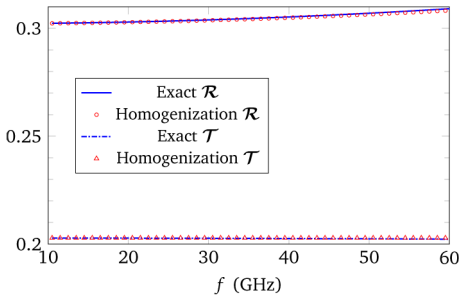

Figure 5. Reflection and transmission coefficients of CFRP, $L = d =$ 0.1 mm, $c = 0.25d$, TM normal incidence.

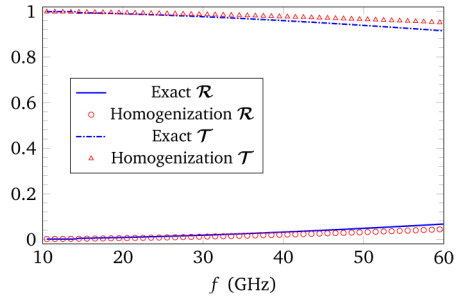

Figure 6. Reflection and transmission coefficients of CFRP, $L = \mathrm{d} =$ 0.1 mm, $c = 0.25d$, TE normal incidence.

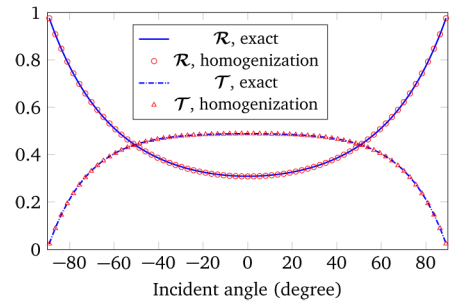

Figure 7. Reflection and transmission coefficients of CFRP, $L = d =$ 0.1 mm, $c = 0.25d$, 60 GHz, TM.

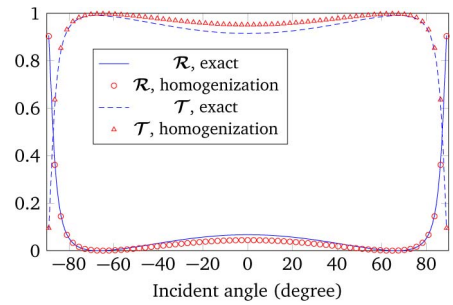

Figure 8. Reflection and transmission coefficients of CFRP, $L = \mathrm{d} =$ 0.1 mm, $c = 0.25d$, 60 GHz, TE.

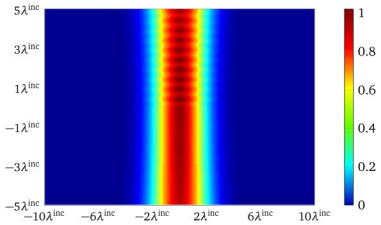

Figure 9. Total field distribution of an E-polarized Gaussian beam normally impinging on the homogenized slab, $L = d = 0.1$ mm, $c = 0.25d$.

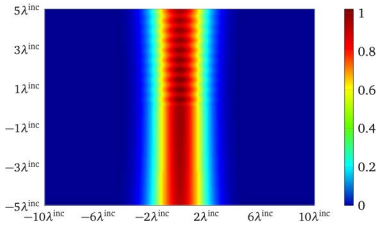

Figure 10. Exact total field distribution; refer to Figure 9.

(increasing with frequency yet still less than 0.04 at 60 GHz), which leads to small absorption of the TE wave.

In addition, the scattering of a Gaussian beam is calculated with the effective permittivity of GFRP. Assume a E-polarized normally incident beam wave with $\lambda^{inc} = 5$ mm, width $\omega_0 = 2\lambda^{inc}$, and center at $x_0 = z_0 = 0$. The field is shown in Figure 9 and the exact one in Figure 10. They match well, and the largest relative error is less than 0.2%.

4. Conclusion

Microstructures of fibered-reinforced polymers influence the behavior of macroscopic fields. Numerical analysis of the response to electromagnetic excitations can lead to a huge amount of memory and CPU if all heterogeneities are finely meshed.

As shown, homogenization ensures high computational efficiency without losing too much accuracy, a single layer being approximated as an equivalent homogeneous slab with effective parameters.

Numerical investigations validate the accuracy of the homogenization, results being compared with those obtained by the analytically rigorous algorithm with good success, especially at low frequency. A certain level of error is observed at relatively high frequency yet well below 4% for all cases considered. This seems tolerable since homogenization is computationally efficient compared to, such as the FDTD and FEM. Once effective parameters are obtained, the macroscopic performance of multilayers with fibers into different directions could be used to replace computationally expensive methods.

5. References

1. B. Cordill, S. Seguin, and M. Ewing, "Shielding Effectiveness of Composite and Aluminum Aircraft,

Model and Measurement Comparison," 2011 IEEE International Instrumentation and Measurement Technology Conference, Hangzhou, China, May 9–12, 2011, pp. 1-5.

2. V. Bui, W. Thitsartarn, E. Liu, J. Chuan, and E. Chua, "EM Performance of Conductive Composite Laminate Made of Nanostructured Materials for Aerospace Application," *IEEE Transactions on Electromagnetic Compatibility*, **57**, 2015, pp. 1139-1148.
3. S. Moy, "Advanced Fiber-Reinforced Polymer (FRP) Composites for Civil Engineering Applications," in N. Uddin (ed.), *Developments in Fiber-Reinforced Polymer (FRP) Composites for Civil Engineering*, Woodhead Publishing Series in Civil and Structural Engineering, Sawston, UK, Woodhead Publishing, 2013, pp. 177-204
4. A. Mehdipour, I. Rosca, A. Sebak, C. W. Trueman, and S. V. Hoa, "Full-Composite Fractal Antenna Using Carbon Nanotubes for Multiband Wireless Applications," *IEEE Antennas and Wireless Propagation Letters*, **9**, 2010, pp. 891-894.
5. J. Su, X. Xu, and B. Hu, "Hybrid PMM-MOM Method for the Analysis of Finite Periodic Structures," *Journal of Electromagnetic Waves and Applications*, **25**, 2011, pp. 267-282.
6. H. Zhang, W. Yin, X. Meng, Z. G. Zhao, H. Zhou, and Y. Liao, "Fast Simulation of Multilayered Anisotropic Carbon Fiber Composite Thin Layers Using the Embedded Thin Layer Model and Improved FDTD Suitable for High Performance Computing," 2018 12th International Symposium on Antennas, Propagation and EM Theory (ISAPE), Hangzhou, China, December 3–6, 2018, pp. 1-4.
7. S. Sádaba, M. Herráez, F. Naya, C. Gonzélez, J. Llorca, and C. Lopes, "Special-Purpose Elements to Impose Periodic Boundary Conditions for Multiscale Computational Homogenization of Composite Materials with the Explicit Finite Element Method," *Composite Structures*, **208**, 2019, pp. 434-441.
8. V. Jandieri, P. Baccarelli, G. Valerio, and G. Schettini, "1-D Periodic Lattice Sums for Complex and Leaky Waves in 2-D Structures Using Higher Order Ewald Formulation," *IEEE Transactions on Antennas and Propagation*, **67**, 2019, pp. 2364-2378.
9. C. Y. Li, D. Lesselier, and Y. Zhong, "Full-Wave Computational Model of Electromagnetic Scattering by Arbitrarily Rotated 1-D Periodic Multilayer Structure," *IEEE Transactions on Antennas and Propagation*, **64**, 2016, pp. 1047-1060.
10. S. Gona and V. Kresalek, "Accuracy of Multilayer Equivalent Models for Composite Laminated Materials," 2009 International Conference on Electromagnetics in Advanced Applications (ICEAA), Turin, Italy, September 14–18, 2009, pp. 694-697.
11. C. Li, *Electromagnetic Modeling and Simulation of Fiber-Reinforced Periodically-Structured Planar Laminates*, Ph.D. dissertation, NNT: 2015PA112219, Université Paris Sud-Paris XI, 2015.
12. X. Meng, P. Sewell, S. Phang, A. Vukovic, and T. Benson, "Modeling Curved Carbon Fiber Composite Structures in the Transmission-Line Modeling Method," *IEEE Transactions on Electromagnetic Compatibility*, **57**, 2015, pp. 384-390.